AIAA Propulsion and Energy Forum
August 9-11, 2021, VIRTUAL EVENT
AIAA Propulsion and Energy 2021 Forum

10.2514/6.2021-3474



# Sensor Integration on Additively Manufactured Hot Section Components for Wireless Gas Turbine Prognostics

Reid A. Berdanier,[1] Scott Fishbone,[2] and Karen A. Thole[3]
*Penn State University, University Park, PA 16802, USA*

Jeffrey Brogan[4]
*CVD MesoScribe Technologies, Central Islip, NY 11722, USA*

Joseph V. Mantese,[5] Thomas J. Martin,[6] and Dustin Caldwell[7]
*Raytheon Technologies Research Center, East Hartford, CT 06108, USA*

Anand Kulkarni[8]
*Siemens Corporation, Charlotte, NC 28273, USA*

Ramesh Subramanian[9]
*Siemens Energy, Orlando, FL 32826, USA*

Benjamin L. Emerson[10] and Timothy C. Lieuwen[11]
*Georgia Institute of Technology, Atlanta, GA 31308, USA*



**To realize the full capability of additively manufactured components in complex energy systems, it is imperative to minimize early component failures during development phases and during operation. Traditional field feedback timelines and offline inspection protocols are insufficient to meet faster-to-market product deployment requirements. Introducing additive manufacturing (AM) approaches can dramatically accelerate development timelines and offers the ability to measure critical parameters in locations that may have been infeasible before given sensor integration requirements. In turn, these measurements can facilitate condition-based operations and maintenance (CBOM) approaches that ultimately lead to reduced operational costs. To fulfill these goals, the current study is developing a method by which to reliably integrate sensors into additively manufactured gas turbine components with applications for both power generation and propulsion. Wireless measurement capabilities are also included as part of the demonstration process through using AM waveguides integral to the tested hardware. A phased demonstration approach is implemented to evaluate sensors deposited on AM parts beginning with simple coupons and increasing in complexity to turbine airfoils and combustor liner hardware. Throughout this approach, considerations of AM surface roughness, sensor performance and durability, and integrated wireless sensing are at the forefront for assessment.**

[1] Assistant Research Professor, Department of Mechanical Engineering, Senior Member AIAA.
[2] Engineering Project Manager, Department of Mechanical Engineering.
[3] Distinguished Professor and Department Head, Department of Mechanical Engineering, Fellow AIAA.
[4] Vice President of Sales and Marketing, CVD Equipment Corporation.
[5] Research Fellow, Physical Sciences Department.
[6] Research Director.
[7] Staff Research Engineer.
[8] Principal Key Expert, Materials and Design in Manufacturing.
[9] Principal Expert, Design for Additive Manufacturing.
[10] Senior Research Engineer, School of Aerospace Engineering, Member AIAA.
[11] Regents Professor and David S. Lewis Jr. Chair, School of Aerospace Engineering, Fellow AIAA.

## I. Introduction

THE United States currently uses approximately 100 Quads of electrical energy per year. Moreover, the US Energy Information Administration (EIA) projects that 97 GW of gas turbine capacity will be installed over the next two decades [1]. To the greatest extent, the present and future source of electrical energy production comes from and will continue to come from turbine-based systems. Concurrently, air travel is expected to double in the next 20 years, in spite of COVID-19 downturns [2], with the majority of air vehicles being turbojet platforms. Thus, by any measure, the importance of stationary power and aero propulsion systems is almost beyond comparison. In addition, the market demand for high efficiency gas turbine engines is ever increasing, thereby requiring faster time-to-market gas turbine products to capture the market share. Furthermore, technologies that maintain uptime, or reduce total cost of ownership, have impact factors that are tremendously multiplied on both a domestic and global basis.

The uses of additive manufacturing (AM) to both develop and produce components for energy conversion systems is already being embraced by many turbine manufacturers due to the potential in revolutionizing current designs and because of the speed at which products can be introduced into the market. The introduction of AM components offers several key advantages: (1) AM can take full advantage of topologically-optimized cooling architectures which are not realized through current casting techniques; (2) AM can improve the component development time by as much as 75% [3]; and (3) AM offers the ability to enable sensor integration in locations that were not previously possible with conventionally cast components, for example. It is important to note, however, that the surface characteristics for an AM component can differ significantly from that of conventionally manufactured components. AM components are inherently rough and that roughness is a strong function of the AM processing parameters, build direction, and post-processing that is available. As such, surface roughness is a key parameter that needs to be considered in sensor integration particularly for direct-write sensor technologies.

The key research questions to be addressed by this work are: *What is the influence of additive manufacturing surface roughness on the deposition success, performance, and durability of direct-write sensors? What is the accuracy and durability of direct-write thermocouples, heat flux sensors, and strain gauges deposited on additively manufactured surfaces?*

## II. Technical Approach

The current effort is developing a manufacturing path that provides an integration approach for sensors into complex turbine components particularly for combustor liners and high pressure turbine airfoils that are operated in extreme environments and temperatures. AM combined with integrated sensors to measure thermomechanical properties will be evaluated to achieve reliable and durable sensing. This approach addresses a major roadblock to innovation of new turbine architectures with additively manufactured components. This roadblock not only affects measurements in operational turbines, but also affects critical measurements needed for turbine development engines and for turbine component testing operated at engine-realistic conditions.

Figure 1 shows an illustration of the relative gains on component lead time that can be achieved through the integration of additively manufactured components instead of traditional cast hardware. These accelerated timelines facilitate faster turnaround of test program results, thereby also enabling more rapid iterations of design improvements. When these components are also created with integrated sensing capability, the influence of design changes can be evaluated more easily, and relevant component durability implications can be extracted from measured parameters.

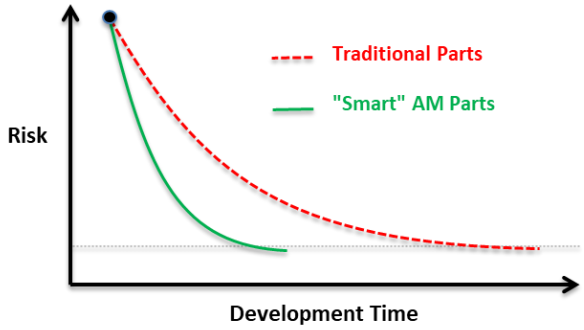


**Figure 1. Development time improvement enabled by introducing AM hardware.**

### A. Substrate Material and Sensor Definition

Inconel 718 (IN718) was selected as the component material for all builds in this study to realize the fundamental understanding of sensor integration into AM components. The application for IN718 in gas turbine engines is widespread – as much as 50% (or more) of typical gas turbine components are manufactured from IN718 for aerospace propulsion applications [4-5]. Moreover, IN718 has been broadly characterized for use in AM processes, and its thermomechanical performance is well known. Past research has explicitly evaluated IN718 as a material for AM turbine blades [6], and other high-temperature applications [7]. Furthermore, IN718 has been used in several preceding projects evaluating heat transfer effects for turbine cooling with an emphasis on AM roughness effects for laser powder bed fusion (L-PBF) [8-13].

Two different additive manufacturing processes are being evaluated in this program. Laser powder bed fusion (L-PBF), such as direct metal laser sintering (DMLS) provides small feature accuracy but, on the other hand, is prohibitively time consuming for the creation of large-scale components. As a result, whereas L-PBF may be advantageous for relatively smaller turbine components for aircraft propulsion purposes, its utility for large-scale power generation turbines may not be advantageous. To address this limitation, directed energy deposition (DED) methods such as laser metal deposition (LMD) provide an alternate approach that can be used to rapidly generate large-scale parts, but at the expense of large feature sizes. Although both methods are under evaluation for this project, only the results from DMLS builds will be presented in this paper.

For our research, sensor deposition is completed using MesoScribe MesoPlasma™ direct write technology. Three different sensor types with application to hot section gas turbine components are being pursued for this study: thermocouples (TC), heat flux sensors (HFS), and strain gauges (SG). Previous work outlining manufacturing and performance of these three sensor types using MesoPlasma™ technology is outlined by Gouldstone et al. [14]. For all sensor types, appropriate ceramic dielectrics are used to electrically isolate sensor materials from the metal component surface. Type N thermocouples were selected due to the nickel-based composition for stability and resistance to oxidation at high temperatures. Heat flux sensors are created by stacking thermocouple junctions separated by dielectric layers to create differential thermopiles. Strain gauges are created by micro-machining a measurement grid into the deposited sensor material (e.g., NiCr).

### B. Coupon Sensor Performance Assessments

This project is following a phased approach of increasing complexity with evaluation of sensor performance in each phase. As an initial step for this research, sensors were deposited externally on flat surface coupons. These first coupon tests provided preliminary assessment of additive surface roughness effects on sensor deposition, but also knowingly created a sensor that protrudes from the component substrate. An ultimate goal for the program is targeting a non-interrupted surface after addition of the sensors. As a result, modified flat surface coupons with trenches were designed, and sensors were deposited in the shallow trenches. Subsequent progressions are advancing the trenched coupon design to more complex curved surfaces representative of turbine vane airfoils.

Past evaluation of direct-write sensors deposited on traditional cast components has defined baseline performance, but the research questions to be answered by this work are focused on performance deviations for additively manufactured hardware relative to this known baseline. To complete sensor performance characterization for additive parts, the following initial steps are completed: measure roughness of AM surface (after post-processing techniques, when appropriate); attempt direct-write sensor deposition process (surface prep, dielectric, sensor, overcoat, etc.); inspect sensor for delamination or other faults; and test sensor for continuity and shorts. If the sensor passes these steps, then it proceeds to a performance assessment phase. Thermocouples are isothermally operated in a tube furnace at a fixed temperature (at least 800°C for this program) and compared with reference thermocouple sensors [14]. Heat flux sensors are thermally cycled by insertion in a heated tube furnace, and then subsequent air cooling after removal from the furnace. The coupon definition for strain gauge tests represents a constant strain cantilever beam, which is then thermally cycled and deflected through a range of prescribed conditions [15].

### C. Wireless Integration and Future Demonstrations

Sensor leads and extension wires are often identified as critical failure points for any instrumented gas turbine component. To circumvent these failure points, a wireless sensor measurement approach is being applied, building upon successful development efforts initially outlined by Attridge et al. [16]. Custom designed RF boards will manage sensor signal and power transmission, and waveguides will be integrated as part of the AM turbine and combustor hardware geometries. Future test programs beyond the scope of this paper will apply the wireless technology and focus on TRL progression with rig-level combustor and turbine demonstrations.

Combustor liner hardware with integrated sensing on AM components will be performed in the Ben T. Zinn Combustion Laboratory at Georgia Tech using cooling geometry defined by Schrager et al. [17-18]. Similarly, turbine hardware demonstrations will be performed in the Steady Thermal Aero Research Turbine (START) Laboratory at Penn State University using turbine vane geometry defined by the National Experimental Turbine (NExT) program [19]. Finally, additional TRL escalation will be achieved through power generation turbine hardware demonstrations performed in partnership with Siemens Energy.

## III. Surface Quality Considerations

A primary concern when utilizing AM techniques is the inherent roughness that is associated with the processes. Specifically focusing on L-PBF methods such as DMLS, a number of studies have shown that roughness can be correlated with build direction, source energy density to build the surface [20] and powder size [21]. However, process parameter control such as contouring [22-23] and hatching [21,24] can also have a significant impact on the roughness. A thorough review of parameters influencing roughness for L-PBF is provided by Snyder and Thole [25] and can be referenced to supplement this non-exhaustive discussion. Synder and Thole also discuss the influence of upskin (supported) and downskin (cantilevered or unsupported) surfaces. A third orientation is considered in the present study, identified as a "sideskin" surface parallel to the build direction, which has also been evaluated recently by Patel et al. [26].

Part-to-part build variations are known to exist for a number of reasons including machine type and process control parameter settings, but also due to less easily identified machine-to-machine differences (i.e., the same type of machine is used with the same parameters, but the build outcome is different due to other circumstances such as non-optimal laser focus). For this reason, specific differentiation is provided in this study for components manufactured from one batch versus another. This identifier (e.g., A, B) is provided in addition to the manufacturing process, which was previously identified as DMLS for all coupons evaluated in this study.

As identified here, effects of roughness due to AM have been well documented. For both internal and external surfaces, post-processing methods for refining roughness have also been evaluated extensively. Some of these post-processing methods have been briefly reviewed by Kumbhar and Mulay [27]. For purposes of this study, two separate post-processing techniques were evaluated as potential options for reducing external surface roughness and improving success rates for sensor deposition and survivability: abrasive grit blasting and ball burnish finish milling.

Surface roughness of AM coupons was quantified using optical profilometry scans. Results from the scans yielded a surface representation in a 2mm x 2mm region. Arithmetic mean surface roughness (Ra) was then calculated from the three-dimensional peaks characterizing the surface relative to the mean surface fit across the same domain. Examples of these scans are shown in Figure 2 for the three different relative build orientations and a subset of surface post-processing techniques. Single-value mean surface roughness (Ra) is provided in Table 1.

An additional column of information in Table 1 also provides a ternary assessment of sensor deposition success rate. In this case, unsuccessful outcomes could be caused by failure modes such as shorted sensor resistance, bondcoat delamination, and other sources leading to unusable products. In general, the higher surface roughness values associated with downskin build coupons were not successful for reasons including bondcoat delamination and sensor resistance short. Several of the sideskin coupons yielded unsuccessful sensor outcomes, despite mean roughness values that were lower than other successful upskin surface coupons. It should be noted, though, that that the failure mode for sensor trials with sideskin coupons (Type I) were markedly different from the shorted resistance type failure mode for high-roughness downskin surfaces (Type VII or VIII). Examples of successful sensor deposition trials are shown in Figure 3(a,b,c) for each of the three sensor types – thermocouple, heat flux sensor, and strain gauge, respectively.

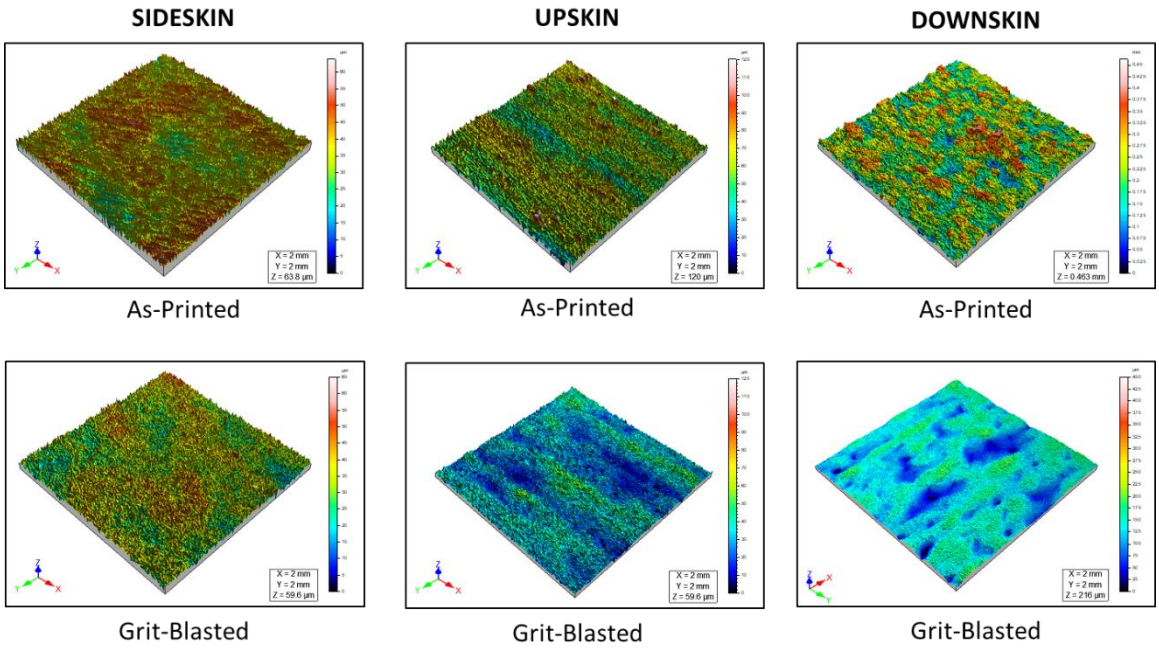


**Figure 2. Example surface roughness scans from optical profilometry for DMLS-A coupons.**

**Table 1. Summary of Measured DMLS Surface Roughness and Associated Sensor Deposition Outcomes**

| Coupon Type | Reference Surface Build Orientation | Manufacturing Process ID | Post-Build Process | Representative Roughness, Ra [μm] | Sensor Deposition Success Rate |
|---|---|---|---|---|---|
| I | Sideskin | DMLS – A | — | 6.7 | Low (1/4) |
| II | Sideskin | DMLS – A | Grit Blast | 5.4 | High (4/4) |
| III | Sideskin | DMLS – B | Grit Blast | 5.2 | High (2/2) |
| IV | Sideskin | DMLS – B | Ball Burnish | 3.1 | High (2/2) |
| V | Upskin | DMLS – A | — | 11 | High (4/4) |
| VI | Upskin | DMLS – A | Grit Blast | 7.3 | High (4/4) |
| VII | Downskin | DMLS – A | — | 48 | Low (1/4) |
| VIII | Downskin | DMLS – A | Grit Blast | 24 | Med (2/4) |

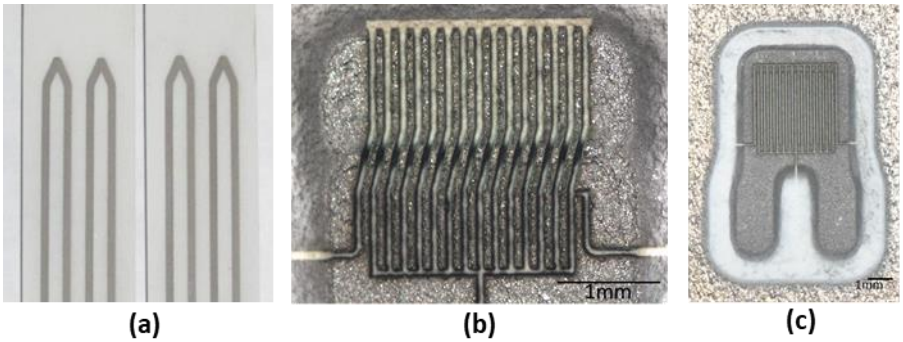


**Figure 3. Example sensor deposition: (a) thermocouples, (b) heat flux sensor, (c) strain gauge.**

As outlined in Table 1, the AM surface roughness has important implications for success of MesoPlasma™ sensor deposition. However, the design of the instrumented surface can also have critical outcomes for the part itself. In particular, use of instrumented hardware components in gas turbine environments can interrupt aerodynamic and thermal boundary layers, leading to inaccurate measurements and undesirable effects on the flowfield itself. This is particularly true if sensors are adhered to the external surface of the component with "standard" unmodified geometry, as illustrated in Figure 4(a). As an alternate approach, post-manufacturing subtractive modifications to the component can be performed to create trenches into which sensors can be integrated, Figure 4(b). Fortunately, the uniqueness of additive manufacturing enables such trenches to be designed into the AM part itself, preventing the need for an additional step to achieve flush-surface sensor integration. Following initial trials of sensor deposition on AM test coupons via external protrusion designs (i.e., Figure 4(a)), program activities performed to date have utilized trenched designs for flush-surface integration (i.e., Figure 4(b)). For reference, all information presented in this paper represent the latter configuration with sensors deposited in trenched geometries.

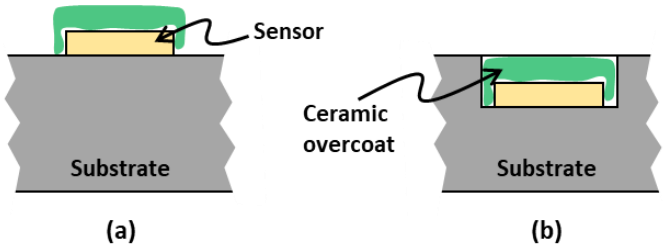


**Figure 4. Sensor integration approaches: (a) external sensor protrusion; (b) flush sensor integration.**

Addressing a desire for flush-surface sensor integration, measurements of the completed sensors were collected using optical profilometry. Figure 5 shows example data from a strain gauge and a thermocouple deposited on two selected coupon types from Table 1. Figure 5(a) shows a microscope image of the completed strain gauge grid using coupon type I as a substrate for analysis, Figure 5(b) shows the corresponding profilometry scan, and Figure 5(c) shows a lateral slice taken at the location identified by the black dashed line in Figure 5(a-b). The height in the lateral slice have been adjusted so that the mean external substrate surface is aligned at a value of zero, yielding a relative height referenced to the external surface. Also in the lateral slice, a dashed red line identifies the peak position of the sensor, as determined by the maximum height in the sensor region; this value is denoted as the sensor peak height, $z_p$. The large-amplitude regions laterally outboard of the sensor region in Figure 5(c) represent ceramic overcoat that extended past the boundaries of the trenched region, as supported by the microscope photo in Figure 5(a). For the strain gauge case shown in Figure 5(a-c), the coated sensor is flush with the adjacent external surface within one micron; in this case, the sensor is slightly below the level of the external surface.

A similar collection of measurements is presented in Figure 5(d-f) for a thermocouple sensor example, as deposited on coupon type IV. The lateral slice data for the thermocouple integration in Figure 5(f) is more representative of the majority of sensor deposition trials performed to date – the sensor peak region protrudes slightly relative to the external surface (typically 100 µm or less), but there is an area adjacent to the sensor itself which is recessed relative to the external surface (also typically 100 µm or less).

Extending this analysis to a full collection of successful sensor deposition trial coupons, Figure 6 compares the relative height difference from the external surface to the sensor peak. All trial coupons show a height difference magnitude between the external surface and the peak sensor surface less than 130 µm; eight of the 11 trials showed a height difference of half that value or less. For all cases except I-SG (discussed previously in Figure 5(a-c)), a positive value of $\Delta z$ indicates a sensor that is protruding past the external surface level. However, Figure 6 also shows that there is no identifiable trend of $\Delta z$ with coupon type (including both build direction and post-processing) or sensor type. Whereas these results are encouraging and show that potential levels of discontinuity between the external surface and the sensor are less than what would be achieved with a true external sensor application (e.g., Figure 4(a)), additional work is required to optimize the trench depth and the overcoating process to achieve the desired results of a true flush-surface application.

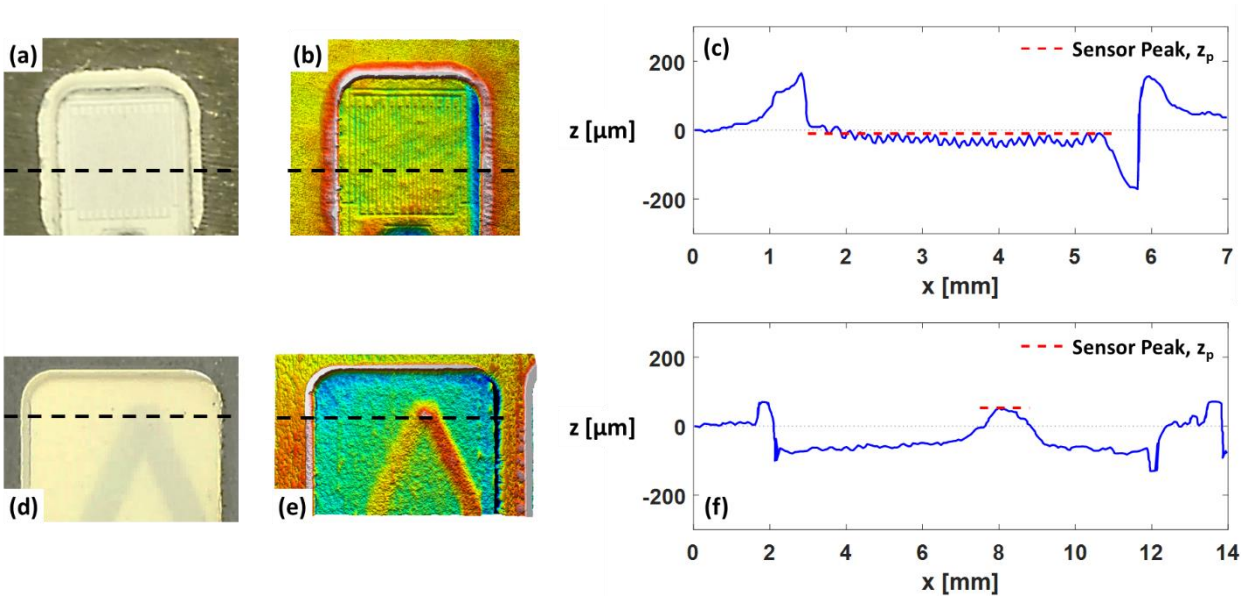


**Figure 5. Selected integrated sensor surface continuity results: (a) I-SG photo; (b) I-SG profilometry scan; (c) I-SG lateral slice; (d) IV-TC photo; (e) IV-TC profilometry scan; (f) IV-TC lateral slice.**

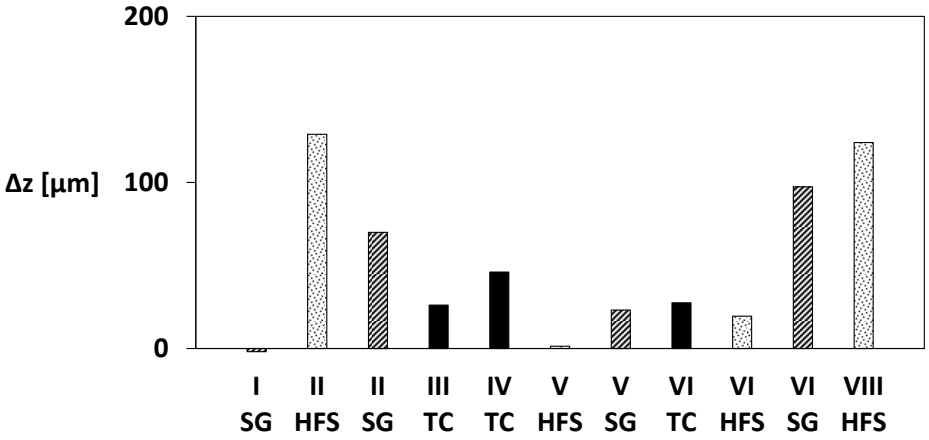


**Figure 6. Relative difference between external surface and peak sensor height for successful sensor deposition trials.**

## IV. Sensor Performance Metrics

For sensors of all types (TC, HFS, and SG), an assessment of sensor performance was performed for successful instrumented components listed in Table 1. The primary targets of these sensor performance assessments have focused on sensor accuracy and durability under harsh conditions up to 800°C and beyond. Figure 7 shows an example test for integrated thermocouples using three different examples spanning two coupon types, III and IV. For thermocouple tests such as the one reported in Figure 7, a Type N MgO reference thermocouple sensor was attached to the component adjacent to the deposited TC sensor. Based on that configuration, the measured sensor error, ε, is calculated as:

$$\varepsilon = T - T_{ref}\,, \tag{1}$$

where T is the measurement from the deposited sensor on the AM substrate, and $T_{ref}$ is the measurement from the adjacent MgO reference thermocouple. This error parameter is presented on the left ordinate in Figure 7 over the course of a 120-hour isothermal test at 800°C. The same results in Figure 7 are also cast as a relative error on the right ordinate:

$$\hat{\varepsilon} = \frac{\varepsilon}{T_{target}} \times 100\ [\%]\ , \tag{1}$$

for which $T_{target}$ is the target value for the test, and all temperature values are cast in absolute terms to yield a dimensionless ratio. The initial heat-up and stabilization period representing approximately 2 hours at the beginning of the 120-hour test was removed for clarity in Figure 7.

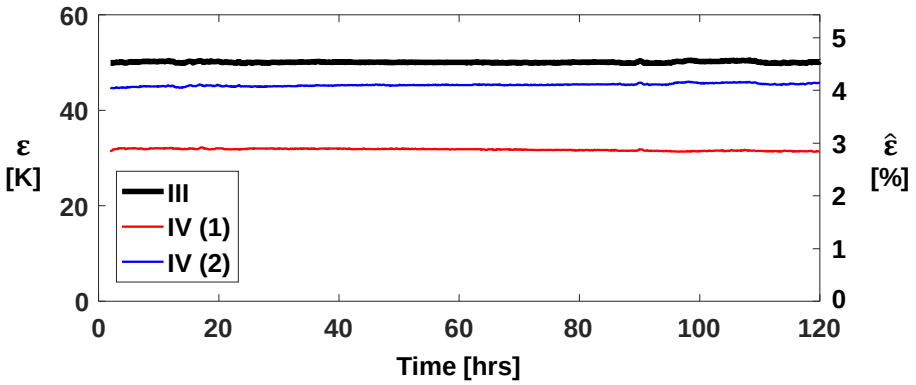


**Figure 7. Type N thermocouple error relative to reference sensor for 120-hour test at 800°C.**

The information in Figure 7 shows bias errors are present for all three sensors when compared with their corresponding reference value – bias errors are less than 50K, or 4.7% relative to the 800°C (1073 K) setpoint. However, this observation is expected, as standard ITS-90 calibration coefficients were applied uniformly, and thin film sensors such as the MesoPlasma™ sensors utilized here exhibit calibrations that can deviate from standard values [28]. Such bias errors are typically be managed in test environments with unique calibrations for the final instrumented hardware assembly, which can significantly reduce thermocouple measurement errors below standard or special limits values, regardless of the size or type of thermocouple. Also in Figure 7, the error values show good stability – all three sensors demonstrate standard deviations better than 0.3K (0.03%) over the 120-hour period. Finally, the drift of printed sensors relative to the reference TC from the beginning of the test to the end of the test is less than 1K (0.1%).

Beyond the 120-hour test outlined in Figure 7, additional trial sensors from earlier phases of this program were evaluated under expanded conditions for longer periods of time (250 hours at 800°C and then subsequently 1100 additional hours at 1000°C). For those expanded test conditions, the measured accuracy reported at 800°C was similarly observed at higher temperatures, with a slight improvement of accuracy (approximately 0.2%) with increased temperature. The observed thermocouple drift over the 1100 hours at 1000°C increased to 2.4% maximum, but that value in particular is negatively impacted by compounding effects from both the higher temperature and the increased duration of the durability assessment trial. Finally, the reproducibility of thermocouple measurement, defined here as the ability to fabricate multiple thermocouple sensors demonstrating the same outputs at specified testing conditions, increased to 0.7% for tests at 1000°C, relative to a value of 0.07% or less at 800°C. It should also be noted that observed values of drift and reproducibility were both negatively impacted most significantly by increases in operating temperature from 900°C to 1000°C, identifying a critical temperature for stability higher than the 800°C target temperature defined for this study. Ultimately, drift and reproducibility represent critical performance metrics; if drift and reproducibility are low, then multiple sensors can be manufactured with the same characteristics, and those characteristics will be stable. As a result, in that situation, calibrations for individual sensors are not required, and general calibration constants can be applied broadly to all sensors from the same fabrication process.

Although thermocouple-based temperature measurements represent a high priority measurement capability for this program, additional evaluations were also conducted to assess performance of heat flux sensors and strain gauges deposited on AM test coupons. Long-term tests of sensor stability and durability for heat flux sensors and strain gauges were performed according to the thermal cycling patterns introduced in section II.B. A combined summary of observed performance parameters for all three sensors is provided in Table 2. Key metrics include: (i) 5% uncertainty (2σ, 95% confidence interval) of measured heat flux characterized by more than 150 thermal cycles up to 800°C; and (ii) strain gauge stability better than 1% (gauge factor) and similar performance to conventional foil strain gauges, as determined from 1000 deflection cycles at 800°C and 24 thermal cycles. Overall, the sensor performance outlined in Table 2 meets or exceeds pre-defined program targets for accuracy and durability.

**Table 2. Summary of Sensor Performance from DMLS Coupon Trials**

| Sensor Type | Metric | Result |
|---|---|---|
| Type N TC | Durability | 120 hours at 800°C |
| | Accuracy | < 6% difference relative to reference |
| | Drift | < 0.1% |
| | Reproducibility | < 0.07% |
| Heat Flux Sensor | Durability | 200+ hours at 800°C |
| | Uncertainty (2σ) | 5% |
| | Sensitivity | > 0.1 mV/W/cm$^2$ |
| Strain Gauge | Durability | > 1000 deflection cycles at ±1100 με |
| | Stability | < 1% gauge factor change |

## V. Conclusions

The utility of AM for gas turbine hardware is well-known for technology development programs, and opportunities for integration with full-scale in-service engines is also on the forefront in several application areas. This program represents a unique approach to advancing gas turbine technology through the application of additively manufactured components with integrated sensors. The ability to monitor components in situ during operation provides invaluable feedback to the design process and toward a growing interest in condition-based operations and maintenance.

Work presented in this study has identified effects of surface roughness, including surface quality driven by build direction and component orientation from the L-PBF processes, and the corresponding impact on MesoPlasma™ deposition of thermocouples, heat flux sensors, and strain gauges. In general, upskin and sideskin surfaces showed notably lower as-built roughness values than downskin surfaces, which aligns with known expectations from other L-PBF studies. Employing post-processing techniques such as grit-blasting and ball burnishing to reduce average surface roughness showed a beneficial impact on the success of sensor deposition processes and the usability of instrumented components. However, even post-processed downskin surfaces still showed decreased likelihood of success relative to upskin or downskin surfaces for the levels of roughness evaluated in this study.

The inherent ability to create customized component geometries through AM provides a valuable opportunity to evaluate flush-surface sensor integration capabilities in tandem with general AM component instrumentation assessments. Trials performed with all three sensor types showed variability in continuity from the mean external surface to the peak sensor surface up to 130 μm. However, even this maximum height difference is an improvement upon the alternate design configuration for sensors deposited on an unmodified external surface. Additional work is underway to refine this step of the process and achieve more repeatable results with fewer surface non-uniformities around the sensor itself.

Finally, the instrumented coupons were tested to assess accuracy and durability of the sensors deposited on AM surfaces. Of particular interest, thermocouple test articles showed bias errors of approximately 50K, which represents less than 5% relative error at the 800°C target temperature. However, the general stability (represented by standard deviation of error) and long-term drift of the sensors were orders of magnitude lower at 0.03% and 0.1%, respectively. Expanded-range assessments up to 1000°C were also conducted for thermocouple sensors to identify potential limitations for excursions beyond the 800°C target temperature – key metrics of accuracy and drift both showed minor performance detriments at the extended range conditions. Similar assessments of heat flux sensor and strain gauge performance showed 5% uncertainty and less than 1% change of gauge factor, respectively.

The results of this study draw the boundaries for a design space supporting sensor deposition on additively manufactured hot section components for gas turbines. This information is contributing to next steps of the project, including topology optimization of combustor and turbine components with hardware modifications to support sensor integration. Future phases of this project include further connection of these sensors to wireless waveguide technology with an ultimate goal to support component-level demonstrations of instrumented AM combustor and turbine test articles with a vision for future integration with next-generation development hardware and fielded engine components.

## Acknowledgments

This material is based upon work supported by the U.S. Department of Energy and Advanced Research Projects Agency–Energy under Award Number DE-AR0001053. This report was prepared as an account of work sponsored by an agency of the United States Government. Neither the United States Government nor any agency thereof, nor any of their employees, makes any warranty, express or implied, or assumes any legal liability or responsibility for the accuracy, completeness, or usefulness of any information, apparatus, product, or process disclosed, or represents that its use would not infringe privately owned rights. Reference herein to any specific commercial product, process, or service by trade name, trademark, manufacturer, or otherwise does not necessarily constitute or imply its endorsement, recommendation, or favoring by the United States Government or any agency thereof. The views and opinions of authors expressed herein do not necessarily state or reflect those of the United States Government or any agency thereof.



## References

[1] U.S. Energy Information Administration, "Annual Energy Outlook 2018," 2018, https://www.eia.gov/outlooks/aeo/.

[2] Pearce, B., "COVID-19: An almost full recovery of air travel in prospect," International Air Transport Association (IATA), 26 May 2021, https://www.iata.org/en/iata-repository/publications/economic-reports/an-almost-full-recovery-of-air-travel-in-prospect/.

[3] Fu, W., Haberland, F., Klapdor, E.V., Rule, D., and Piegert, S., "Streamlined Frameworks for Advancing Metal Based Additive Manufacturing Technologies in Gas Turbine Industry," GPPF-2017-182, 2017.

[4] Schafrik, R.E., Ward, D.D., and Groh, J.R., "Application of Alloy 718 in GE Aircraft Engines: Past, Present, and Next Five Years," *Proceedings of Superalloys 718, 625, 706 and Various Derivatives*, The Minerals, Metals & Materials Society, 2001, pp. 1-11.
doi: 10.7449/2001/Superalloys_2001_1_11

[5] Paulonis, D.F. and Schirra, J.J., "Alloy 718 at Pratt & Whitney – Historical Perspective and Future Challenges," *Proceedings of Superalloys 718, 625, 706 and Various Derivatives*, The Minerals, Metals & Materials Society, 2001, pp. 13-23.
doi: 10.7449/2001/Superalloys_2001_13_23

[6] Caiazzo, F., Alfieri, V., Corrado, G., and Argenio, P., "Laser powder-bed fusion of Inconel 718 to manufacture turbine blades," *Int. J. Adv. Manuf. Technol.*, Vol. 93, 2017, pp. 4023-4031.
doi: 10.1007/s00170-017-0839-3

[7] Yong, C.K., Gibbons, G.J., Wong, C.C., and West, G., "A Critical Review of the Material Characteristics of Additive Manufactured IN718 for High-Temperature Application," *Metals*, Vol. 10, 2020, pp. 1576.
doi: 10.3390/met10121576

[8] Snyder, J. C., Stimpson, C. K., Thole, K. A., Mongillo, D. J., "Build Direction Effects on Microchannel Tolerance and Surface Roughness," *J. Mech. Des.*, Vol. 137, No. 11, 2015, pp. 111411.
doi: 10.1115/1.4031071

[9] Snyder, J. C., Stimpson, C. K., Thole, K. A., and Mongillo, D., "Build Direction Effects on Additively Manufactured Channels," *J. Turbomach.*, Vol. 138, No. 5, 2016, pp. 051006
doi:10.1115/1.4032168.

[10] Stimpson, C. K., Snyder, J. C., Thole, K. A., and Mongillo, D., "Roughness Effects on Flow and Heat Transfer for Additively Manufactured Channels," *J. Turbomach.*, Vol. 138, No. 5, 2016, pp. 051008.
doi:10.1115/1.4032167

[11] Stimpson, C. K., Snyder, J. C., Thole, K. A., and Mongillo, D., "Scaling Roughness Effects on Pressure Loss and Heat Transfer of Additively Manufactured Channels," *J. Turbomach.*, Vol 139, No. 2, 2017, pp. 021003.
doi: 10.1115/1.4034555

[12] Ferster, K. K., Kirsch, K. L., and Thole, K. A., "Effects of Geometry, Spacing, and Number of Pin Fins in Additively Manufactured Microchannel Pin Fin Arrays," *J. Turbomach.*, Vol. 140, No. 1, 2017, p. 011007.
doi: 10.1115/1.4038179

[13] Wildgoose, A. J., Thole, K. A., Sanders, P., Wang, L., "Impact of Additive Manufacturing on Internal Cooling Channels with Varying Diameters and Build Directions," ASME GT2020-15049, 2020.
doi: 10.1115/GT2020-15049

[14] Gouldstone, C., Gutleber, J., and Smith, W., "Direct-Write Strain and Temperature Sensors for Harsh Environments," *AIP Conference Proceedings*, Vol. 894, 2007, pp. 949-956.
doi: 10.1063/1.2718070

[15] Gouldstone, C., Brogan, J., Greenlaw, R., Gambino, R.J., Gutleber, J., Sampath, S., and Longtin, J., "Embedded resistive strain sensors for harsh environments," *IEEE Aerospace Conference*, 2006.
doi: 10.1109/AERO.2006.1656094

[16] Attridge, P., Bajekal, S., Klecka, M., Wu, X., Savulak, S., Viens, D., Carey, M., Miano, J., Rious, W., Zacchio, J., Dunst, R., Straug, D., Mantese, J., "Additively Manufactured IN718 Components with Wirelessly Powered and Interrogated Embedded Sensing," DOE Award DE-FE0012299, Final Technical Report, 2015.
doi: 10.2172/1369567

[17] Shrager, A., Thole, K. A., and Mongillo, D., "Effects of Effusion Cooling Pattern Near the Dilution Hole for a Double-Walled Combustor Liner – Part 1: Overall Effectiveness Measurements", *Journal of Engineering for Gas Turbines and Power*, Vol. 141, No. 1, 2019, pp. 011022.
doi: 10.1115/1.4041148

[18] Shrager, A., Thole, K. A., and Mongillo, D., "Effects of Effusion Cooling Pattern Near the Dilution Hole for a Double-Walled Combustor Liner – Part 2: Flowfield Measurements", *Journal of Engineering for Gas Turbines and Power*, Vol. 141, No. 1, 2019, pp. 011023.
doi: 10.1115/1.4041153

[19] Thole, K.A., Barringer, M.D., Berdanier, R.A., Fishbone, S., Wagner, J.H., Dennis, R., Black, J., Burke, P., Straub, D., O'Neill, F., Stimpson, C.K., Riahi, A., Aggarwala, A., Bradshaw, S., Kohli, A., Mongillo, D., Praisner, T., Rodriguez, J., Fox, M., and Kim, Y.W., "Defining a Testbed for the U.S. Turbine Industry: The National Experimental Turbine (NExT)," AIAA Propulsion & Energy Forum, 2021.

[20] Wang, L-Z., Wang, S., and Wu, J.-J., "Experimental investigation on densification behavior and surface roughness of AlSi10Mg powders produced by selective laser melting," *Optics & Laser Technology*, Vol. 96, 2017 pp. 88-96.
doi: 10.1016/j.optlastec.2017.05.006

[21] Kudzal, A., McWilliams, B., Hofmeister, C., Kellogg, F., Yu, J., Taggart-Scarff, J., and Liang, J., "Effect of Scan Pattern on the Microstructure and Mechanical Properties of Powder Bed Fusion Additive Manufactured 17-4 Stainless Steel," *Materials & Design*, Vol. 133, 2017, pp. 205–215.
doi: 10.1016/j.matdes.2017.07.047

[22] Fox, J. C., Moylan, S. P., and Lane, B. M., "Effect of Process Parameters on the Surface Roughness of Overhanging Structures in Laser Powder Bed Fusion Additive Manufacturing," *Procedia CIRP*, Vol. 45, 2016, pp. 131–134.
doi: 10.1016/j.procir.2016.02.347

[23] Koutiri, I., Pessard, E., Peyre, P., Amlou, O., and De Terris, T., 2018, "Influence of SLM Process Parameters on the Surface Finish, Porosity Rate and Fatigue Behavior of as-Built Inconel 625 Parts," J. Mater. Process. Technol., Vol. 255, May, 2018, pp. 536–546.
doi: 10.1016/j.jmatprotec.2017.12.043

[24] DePond, P. J., Guss, G., Ly, S., Calta, N. P., Deane, D., Khairallah, S., and Matthews, M. J., "In Situ Measurements of Layer Roughness during Laser Powder Bed Fusion Additive Manufacturing Using Low Coherence Scanning Interferometry," *Materials & Design*, Vol. 154, 2018, pp. 347–359.
doi: 10.1016/j.matdes.2018.05.050

[25] Snyder, J.C. and Thole, K.A., "Understanding Laser Powder Bed Fusion Surface Roughness," *J. Manuf. Sci. Eng.*, Vol. 142, No. 7, 2020, 071003.
doi: 10.1115/1.4046504

[26] Patel, S., Rogalsky, A., and Vlasea, M., "Towards understanding side-skin surface characteristics in laser powder bed fusion," J. Materials Research, Vol. 35, No. 15, 2020, pp. 2055-2064.
doi: 10.1557/jmr.2020.125

[27] Kumbhar, N.N. and Mulay, A.V., "Post processing methods used to improve surface finish of products which are manufactured by additive manufacturing technologies: A review," *J. Inst. Eng. India Ser. C*, Vol. 99, No. 4, 2018, pp. 481-487.
doi: 10.1007/s40032-016-0340-z

[28] Siroka, S., Berdanier, R.A., Thole, K.A., Chana, K.S., Haldeman, C.W., and Anthony, R.J., "Comparison of Thin Film Heat Flux Gauge Technologies Emphasizing Continuous-Duration Operation," *J. Turbomachinery*, Vol. 142, No. 9, 2020, pp. 091001.
doi: 10.1115/1.4045991